

See discussions, stats, and author profiles for this publication at: <https://www.researchgate.net/publication/255762499>

First principles calculations of solid–solid interfaces: An application to conversion materials for lithium–ion batteries

Article in *Journal of Materials Chemistry* · October 2012

DOI: 10.1039/C2JM35078E

CITATIONS

37

READS

357

5 authors, including:



Germain Vallverdu

Université de Pau et des Pays de l'Adour

46 PUBLICATIONS 857 CITATIONS

[SEE PROFILE](#)



Herve Martinez

Université de Pau et des Pays de l'Adour / Centrale Casablanca (MAROC)

231 PUBLICATIONS 7,181 CITATIONS

[SEE PROFILE](#)



Frédéric Le Cras

Atomic Energy and Alternative Energies Commission

149 PUBLICATIONS 5,197 CITATIONS

[SEE PROFILE](#)



Isabelle Baraille

Université de Pau et des Pays de l'Adour

89 PUBLICATIONS 2,337 CITATIONS

[SEE PROFILE](#)

First principles calculations of solid-solid interfaces : application to conversion materials for lithium-ion batteries

L. Martin * † G. Vallverdu †‡ H. Martinez† F. Le Cras* I. Baraille†

August 31, 2012

Abstract

Using periodic density functional theory approaches, the thermodynamic stability of solid-solid interfaces generated during the conversion reaction of copper oxide which is a promising electrode material is investigated. Previous experimental results showed that conversion reactions generate a huge proportion of solid-solid interfaces among Cu₂O–Cu, Li₂O–Cu and Cu₂O–Li₂O. Interface grand potentials as a function upon the voltage against a Li|Li⁺ were computed in order to determine the chemical composition of the most stable interfaces. Then a structural model of the electrode material is proposed, based on the work of adhesion of the most stable systems identified in the first step.

Keywords : solid-solid interface, first principles calculations, conversion materials, Li-ion batteries, Electrode morphology, copper oxide

1 Introduction

Although computational approaches are widely used in material science, solid-solid interface studies are still challenging issues because of the computational cost and the difficulty to build relevant models or to merge different formalisms in order to obtain an accurate description of each phases composing the interface. Nevertheless, interfacial effects play a dominant role in many applications such as composite materials, transistors... Reliable and precise data whether at the structural or chemical level are often obtained with difficulty from experimental techniques. Their low thickness, their possible reactivity and their difficulty of access from bulk or surface techniques explain that few experimental works report data on solid/solid interfaces. Theoretical approaches are then interesting tools^{1–4} and have been successfully applied for example to metal/ceramic interface and wetting^{5–7} or to conversion materials for Li-ion batteries.^{8–10} In these studies, periodic calculations at a Density Functional Theory (DFT) level are

used in order to compute interface formation energies or works of adhesion and separation which could be compared, in a Yound-Dupré formalism, to wetting experiments.

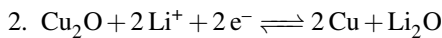
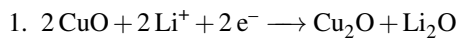
Intense research efforts are made in the field of Li-ion batteries to satisfy the growing need for highly efficient power sources suitable for numerous devices (micro-electronics, transportation ...). The performances (reversible capacity and the cycle life) of such systems are closely linked to complex phenomena occurring at the electrode/electrolyte interface, including the formation of the solid electrolyte interphase (SEI) layers.¹¹ For lithium microbattery, which consists of a monolithic electrochemical system constituted of several stacked layers (thin films) including the active part (both electrodes and electrolyte), current collectors, insulating and lithium diffusion barrier layers, thin film encapsulation, which total thickness does not exceed 15 μm, solid-solid interfaces represent a crucial issue for optimal performances. Furthermore, to enhance the energy density of Li-ion cells, the improvement of electrode materials has led to the investigation of conversion materials¹² (transition metal oxides for example) instead of traditional intercalation compounds. Conversion materials present spectacular capacities corre-

*CEA LITEN, 17 Rue des Martyrs, F-38054 Grenoble, France

†Université de Pau et des Pays de l'Adour, IPREM - ECP CNRS UMR 5254, Hélioparc Pau-Pyrénées, 2 av. du Président Angot, 64053 Pau cedex 9, France

‡Corresponding Author germain.vallverdu@univ-pau.fr

lated with the complete reduction of a metal oxide into a composite electrode consisting of nano-sized metallic particles embedded into a Li_xO matrix.^{13,14} Thus, several phases are generated during the electrochemical cycles and there is a substantial surface area of solid-solid interfaces in the electrode at a nano scale. New theoretical approaches in the field of solid-solid interfaces of conversion electrodes thus represent interesting tools to better understand the behavior of the material during electrochemical cycles. The objective of this paper is to study the interfaces generated during an electrochemical cycle, by taking cupric oxide CuO as an example. Among the metal oxides used as conversion materials, CuO is well known in the battery community because it acts as positive electrode material in primary $\text{CuO}|\text{Li}$ cells available on the market, which operates between 1.4 and 1.0 V. Since Tarascon *et al.* first reported the reversible lithium conversion reactivity of CuO particles,^{15,16} copper (II) oxide appears as an attractive material because of its low cost, non toxicity and high theoretical specific capacities (674 mAh.g⁻¹ and 4260 mAh.cm⁻³). The first reduction of a CuO electrode (Li^+ insertion) is a two steps conversion process :



At the end of the first discharge, the electrode is composed of metallic copper and Li_2O . At the end of the first charge (Li^+ extraction), CuO is not formed again.¹⁶ Redox processes stop after the step 2 and the electrode contains Cu_2O and Li_2O phases. Note that LiCuO_2 , Li_2CuO_2 and LiCu_2O_2 are well characterized phases¹⁷ but were not considered in the present paper as CuO was examined as a conversion electrode and not as an insertion one.

In this paper, we investigate the solid-solid interfaces generated during the conversion step of Cu_2O into Cu and Li_2O , *i.e.* $\text{Cu}_2\text{O}-\text{Cu}$, $\text{Li}_2\text{O}-\text{Cu}$ and $\text{Cu}_2\text{O}-\text{Li}_2\text{O}$ interfaces, by means of periodic DFT calculations in order to identify the most stable interfaces and to suggest a structural model of the electrode during the electrochemical cycle. First we will describe the methodology used to build interface models and the thermodynamic approach undertaken in order to investigate the relative stability of the interface models. Then, preliminary results needed to build the interface models will be presented and their relative stability will be discussed.

Finally, a structure of the electrode material will be proposed.

2 Computational methodology and models

2.1 Interface model construction

Considering two phases A and B, several steps have to be done in order to build an interface model. They are summarized on Figure 1. First, the interface plane between A and B has to be chosen to determine the stacking direction. Second, in this direction the bulk phases of A and B have to commensurate in order to build a 2D periodic interface model. The third step consists of the cleavage of the bulks. During this step, the last atomic layer at the surface of each phase is selected and depending on the chemical composition of the system, several surfaces can be obtained. Finally, in the fourth step, an abrupt interface model is built by bringing together two surfaces of phase A and B, and then the whole system is fully relaxed. The chemical composition of the interface is determined during the cleavage step by the choice of the surface of each phase which will be face to face.

2.1.1 Bulk phases and stacking direction

The Cu_2O , Li_2O and Cu bulks are cubic lattices with cell parameter a_c : Cu ($Fm\bar{3}m$, $a_c = 3.620 \text{ \AA}$)¹⁸; Li_2O antifluorine structure ($Fm\bar{3}m$, $a_c = 4.619 \text{ \AA}$)¹⁸; Cu_2O ($Pm\bar{3}n$, $a_c = 4.271 \text{ \AA}$)¹⁹ with copper atoms on a fcc sublattice and oxygen atoms on one quarter of the tetrahedral sites.

As each phase presents atoms on a fcc lattice the [111] direction is a convenient stacking direction and interface models were built perpendicularly to this direction. Thermodynamic surfaces stability of Cu_2O and Li_2O was experimentally and theoretically investigated in literature²⁰⁻²³ and it was shown that (111) surfaces are the most stable. In the case of Cu_2O , (111) surface exhibits the lowest surface free energy whatever the oxygen conditions of the environment²⁰ and no reconstruction was observed experimentally.²¹ In the case of Li_2O , the most stable surface is also the (111) surface with a Li termination.^{22,23}

Note that the existence of an interface formation perpendicular to the [111] direction was already observed experimentally by Kunze *et al.*²⁴ Starting from

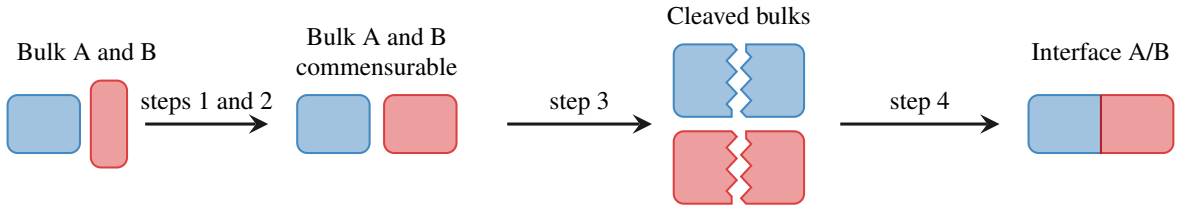


Figure 1: Successive steps leading to an interface model from two bulk phases A and B.

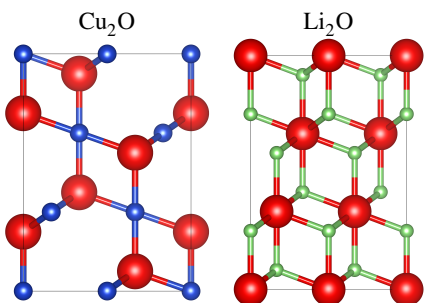


Figure 2: Bulk structures in the $2 \times 2 \times 1$ hexagonal supercell. The projection in the $(\bar{2}\bar{1}0)$ plane of the hexagonal lattice highlights the three layers structure. Oxygen atoms are red, lithium atoms green and copper atoms blue.

a Cu(111) surface, they made a Cu_2O phase to grow up by an oxidation procedure upon the Cu surface. They showed that the orientation of the Cu_2O lattice is the same as the Cu lattice, namely the Cu_2O surface is perpendicular to the [111] direction and there is not in plane rotation of the Cu_2O lattice relatively to the Cu lattice.

In the [111] direction, the unit cell of each bulk is hexagonal, see Figure 2. In the case of Cu_2O , oxygen atoms are not on a fcc sub-lattice (space group $Pm\bar{3}n$), thus, in order to keep the stoichiometry and the periodicity of Cu_2O in the hexagonal lattice a $2 \times 2 \times 1$ supercell has to be used. As a consequence, $2 \times 2 \times 1$ supercells were used for all lattices to build the interface models. In the following, the parameters of the $2 \times 2 \times 1$ hexagonal supercell of the bulk phases will be called a_h and c_h ($a_h = a_c\sqrt{2}$, $c_h = a_c\sqrt{3}/2$ where a_c is the cubic lattice parameter).

2.1.2 Commensurability of two phases

One issue to build an interface model is to make the phases composing the interface to commensurate. The mismatch, σ is related to the disparity between two phases and reads²⁵

$$\sigma = 1 - \frac{2S_{A-B}}{S_A + S_B} \quad (1)$$

where S_A and S_B are respectively the surface areas of the A and B unit cells and S_{A-B} is the overlapping surface area. Using experimental lattice parameters (a_h is equal to 6.04 Å for Cu_2O , 5.12 Å for Cu and 6.53 Å for Li_2O) mismatches of 24%, 16% and 8% are obtained for the $\text{Li}_2\text{O}-\text{Cu}$, $\text{Cu}_2\text{O}-\text{Cu}$ and $\text{Cu}_2\text{O}-\text{Li}_2\text{O}$ interfaces respectively.

In the literature two different approaches are used in order to ensure the commensurability of two phases. In the first one, called the (1×1) model, only one unit cell is used in the plane of the interface. Lattice parameters are scaled until a perfect matching of the two lattices of the phases composing the interface is reached and an atomically coherent interface model is built. This method is used in the largest part of *first principles* studies of interface models^{6-8,10,26,27} and suits well for phases with a relatively small mismatch.

The second approach consists of determining a ratio of two integers q and p closed to the ratio of lattice parameters in the interface plane. Then, the interface model is built from two supercells, namely $p \times p$ for one phase and $q \times q$ for the other. This strategy leads to incoherent or semi-coherent interface models with minimized mismatch.²⁸ The stress energy needed for the construction of the interface model is relatively small and interface models built from phases with a large disparity in their lattice parameters can be investigated. Nevertheless, such interface models are too huge and may be not suited in order to carry out a complete *first principles* study.

For example, in the case of Cu and Cu₂O phases, the ratio between the a_h parameters is ~ 0.84 and could be approximated by 4/5. Thus, an interface model (4×4)Cu₂O/(5×5)Cu with supercell parameters equal to 24.2 Å and 25.6 Å for Cu₂O and Cu respectively, leads to a mismatch of $\sim 5.6\%$ (instead of 16% in the 1×1 model). Such a model contains at least 588 atoms and is too huge for the investigation of numerous interfaces with *first principles* techniques. Both approaches were compared by Wang *et al.*²⁸ in a study of Si/Cu interfaces perpendicular to the [111] direction where the mismatch between Si and Cu is about 35%. They showed that even with a large stress energy, a full relaxation of a 1×1 interface model only overestimates the separation work obtained for the (2×2)Si/(3×3)Cu model by $\sim 3\%$.

Consequently, the 1×1 model was used in our work. The strategy used in order to determine the common value of a_h for each couple of phase is presented in the results section.

2.1.3 The interface model

The interface models between phase A and B were built in the same way as slab models for surface calculations. They consist of a symmetric supercell with several layers of each phases which form two slabs, perpendicular to the [111] direction of the bulks. All models are symmetric with respect to the center of the supercell in order to avoid long-range dipole-dipole interactions. Thus, two identical interfaces appear in each models. For each phase, we selected a number of atomic layers such as the distance between two interfaces was greater than 12 Å in order to avoid non physical interactions between the interfaces and to preserve bulk properties in the inner layers.

Along the [111] direction, Li₂O and Cu₂O phases consist of a stacking of Li-O-Li or O-Cu-O three layers respectively, see Figure 2. The chemical composition of the interface is determined by the choice of the last atomic layer of each cleaved bulk which will be packed into the interface model. Thus, three different models can be built for Li₂O–Cu and Cu₂O–Cu interfaces and nine for Cu₂O–Li₂O interfaces. In order to specify the chemical composition at the interface, interface models will be called (A)X-Y(B) where A and B are the phases composing the interface and X and Y are respectively the atoms composing the last atomic layer of parts A and B. The A-B notation will stand for the general case including all possible chemical com-

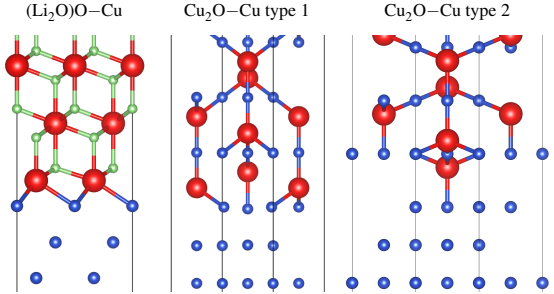


Figure 3: (Li₂O)-Cu interface (left picture), Cu₂O–Cu type 1 interface (central picture) and Cu₂O–Cu type 2 interface (right picture).

positions. For example, the interface between Li₂O and Cu with an oxygen atomic layer at the end of the Li₂O part will be called (Li₂O)-Cu and is presented Figure 3. Cu₂O–Cu interfaces lead to two different models called type 1 and type 2 presented Figure 3. If the three layers structure of Cu₂O or Li₂O phases is broken in the cleavage step, the stoichiometry of these phases is not conserved during the interface formation and the investigation of the relative thermodynamic stability of interface models needs a specific treatment.

2.2 Thermodynamic approach

For each couple of phases, the most stable chemical composition of the interface is determined following a thermodynamic approach. To compare the relative stability of the models with different chemical compositions, a thermodynamic grand canonical ensemble treatment is required. In such an ensemble, all models are assumed to be in chemical and thermal equilibria with bulk phases and the relevant thermodynamic quantity is the grand potential Ω .⁵ At this point, we assume that the entropic and volumetric contributions to the grand potential are negligible. Thus, for an interface between phases A and B, the grand potential reads

$$\Omega_{A-B} = \frac{1}{2S_{A-B}} \left[E_{A-B}^i - \sum_{j \in A-B} N_j \mu_j \right] \quad (2)$$

where S_{A-B} is the area of the interface, E_{A-B}^i is the energy of the interface model after a full relaxation of the system and N_j and μ_j are the number of atoms and the chemical potential of the j species, among {Cu, Li, O}, composing the interface model. The factor 2 comes

from the fact that each system contains two identical interfaces because of the symmetry of each model.

The chemical equilibria between bulk phases A and B and the interface A-B leads to

$$\begin{cases} E_A^b = \sum_{j \in A} N_j \mu_j \\ E_B^b = \sum_{j \in B} N_j \mu_j \end{cases} \quad (3)$$

where E_A^b and E_B^b are the DFT energies of bulk phases A and B respectively. As a consequence, for ternary systems such as $\text{Li}_2\text{O}-\text{Cu}$ and $\text{Cu}_2\text{O}-\text{Li}_2\text{O}$ interfaces, there are two phases and two chemical equilibria and the phase rule requires that only one chemical potential is independent. Except in the case of binary systems such as $\text{Cu}_2\text{O}-\text{Cu}$ where chemical potentials are completely determined, $\Delta\mu_{\text{Li}} = \mu_{\text{Li}} - \mu_{\text{Li}}^*$ was chosen as the independent variable. μ_{Li}^* is the chemical potential of lithium in its standard state²⁹ which is approximated by the bulk DFT energy of Li metal, E_{Li}^b . Because metallic Li was chosen as the reference state, the scale of $\Delta\mu_{\text{Li}}$ translates directly into the negative of the voltage against $\text{Li}|\text{Li}^+$. Combining equations (2) and (3), grand potentials read

$$\Omega_{\text{Li}_2\text{O}-\text{Cu}} = \frac{1}{2S} \left[E_{\text{Li}_2\text{O}-\text{Cu}}^i - N_{\text{Cu}} E_{\text{Cu}}^b - N_{\text{O}} E_{\text{Li}_2\text{O}}^b + (2N_{\text{O}} - N_{\text{Li}}) \Delta\mu_{\text{Li}} + (2N_{\text{O}} - N_{\text{Li}}) E_{\text{Li}}^b \right] \quad (4)$$

$$\Omega_{\text{Cu}_2\text{O}-\text{Li}_2\text{O}} = \frac{1}{2S} \left[E_{\text{Cu}_2\text{O}-\text{Li}_2\text{O}}^i - \frac{N_{\text{Cu}}}{2} E_{\text{Cu}_2\text{O}}^b - (N_{\text{O}} - \frac{N_{\text{Cu}}}{2}) E_{\text{Li}_2\text{O}}^b - (N_{\text{Cu}} + N_{\text{Li}} - 2N_{\text{O}}) \Delta\mu_{\text{Li}} - (N_{\text{Cu}} + N_{\text{Li}} - 2N_{\text{O}}) E_{\text{Li}}^b \right] \quad (5)$$

$$\Omega_{\text{Cu}_2\text{O}-\text{Cu}} = \frac{1}{2S} \left[E_{\text{Cu}_2\text{O}-\text{Cu}}^i - N_{\text{O}} E_{\text{Cu}_2\text{O}}^b - (N_{\text{Cu}} - 2N_{\text{O}}) E_{\text{Cu}}^b \right] \quad (6)$$

Except for $\text{Cu}_2\text{O}-\text{Cu}$ interfaces, all grand potentials Ω_i depend linearly upon $\Delta\mu_{\text{Li}}$. In the specific case of stoichiometric models, the coefficient of $\Delta\mu_{\text{Li}}$ in equations (4), (5) and (6) is equal to zero, thus grand potentials are constant which is consistent with a canonical situation.

The range of meaningful chemical potentials is determined by considering the region of the phase diagram of $\{\text{Cu}, \text{O}, \text{Li}\}$ where bulk phases Cu_2O , Li_2O and Cu are stable and coexist, see the result section.

Since in the interface models, bulk phases are distorted in order to obtain a perfect matching of the lattices, $\Omega_{\text{A}-\text{B}}$ includes explicitly the stress energy contribution. The calculation of the real stress energy is not straightforward because phenomena such as dislocations or defects which could appear during the compression or the expansion of the material, are unknown. The accurate evaluation of such phenomena is not the subject of this study. In the following, the DFT energies of bulks will be substituted by DFT energies of distorted bulks corresponding to the same a_h and c_h parameters as in the interface model.⁶ As a consequence, in equations (4), (5) and (6) the same stress energy is contained in DFT energies of the interface model and the distorted bulks and would therefore cancel. Grand potentials computed in this way only include the energies of the chemical contributions to the interface formation.

2.3 Computational details

All calculations were performed using the plane wave DFT code available in the Vienna Ab Initio Simulation Package (VASP)^{30,31} within the generalized gradient approximation, using PBE functional.³² The electronic wave-functions were described in the Projected Augmented Wave (PAW) formalism^{33,34} and a realspace projection was further used for the total wavefunction analysis. DFT+U calculations were done using the rotationally invariant approximation of Dudarev *et al.*³⁵ in which the onsite Coulomb parameter U and the exchange parameter J are combined into a spherically averaged, single effective interaction parameter. Hereafter we will refer to the $U - J$ effective parameter as U . There is a methodological issue arising from the fact that we have to describe simultaneously a metallic compound (here copper) and an insulator (here Cu_2O). The first one is well described by a simple DFT calculation whereas the last one needs self-interaction corrected methods such as DFT+U or hybrid functionals. In this work, in the case of $\text{Cu}_2\text{O}-\text{Cu}$ and $\text{Cu}_2\text{O}-\text{Li}_2\text{O}$ interface models, a self-interaction correction was added on copper atoms belonging to the Cu_2O part whereas no correction was added on copper atom belonging to the copper metallic part. Two different values of the U parameter were adopted, namely $U = 6.5$ eV and $U = 4$ eV. The former determined by Anisimov *et al.*^{36,37}

has been already used in previous studies of copper oxides.^{38–40} The second was fitted by Wang *et al.*⁴¹ in order to give the best agreement with reaction enthalpies. In the case of Li₂O, simple DFT calculations are accurate enough because of the large gap in this system (~ 5 eV) and the lack of 3d electrons. Bader decomposition of charge density was used to determine atomic charges^{42,43} using a finer grid for the electronic density, namely, around $\Delta x = 0.03 \text{ \AA}$.

We checked the quality of the basis set by increasing the plane wave energy cut-off from 400 to 600 eV in bulk calculations of phases Cu, Cu₂O and Li₂O. The plane wave energy cut-off was set to 520 eV which is a converged value corresponding to 1.3 times the cut-off energy set in VASP oxygen pseudo-potentials and was already used in previous works on bulk and surface calculations of Cu₂O.⁴⁴ The Brillouin zone integration was done on a k -point grid distributed uniformly around the origin using a mesh of $6 \times 6 \times 6$ for all bulk calculations and a mesh of $6 \times 6 \times 1$ for all interface or surface calculations. Ionic relaxations are done in two steps to avoid Pulay stress. First, only atomic positions are relaxed and then a full relaxation of the structure is done. Structure are minimized until the forces acting on each atom were less than $0.01 \text{ eV} \cdot \text{\AA}^{-1}$. Ionic relaxations were done using the DFT formalism. Single point calculations using the DFT+ U formalism and a spin polarized electronic density were done on the relaxed structures.

3 Results and discussion

3.1 Bulk phases and phase diagram

Bulk phase calculations were used in order to check the reliability of our computational parameters and to build the phase diagram of {Cu, O, Li} from which we identified meaningful limits of $\Delta\mu_{\text{Li}}$. Table 1 presents the lattice parameters and bader charges obtained after a full relaxation of bulk phases in their hexagonal lattice. Lattice parameters agree well with experimental data. The optimized values show a deviation of less than 1% from the experimental ones. Bader charges are in good agreement with previous calculations on Cu₂O⁴⁵ and Li₂O.⁴⁶ These results will be used as a reference in the analyses of interface structures.

The phase diagram of {Cu, O, Li}, Figure 4, was built as done by Kramer *et al.*⁴⁷ using $\Delta\mu_{\text{O}} = \mu_{\text{O}} - \mu_{\text{O}}^*$ and $\Delta\mu_{\text{Li}} = \mu_{\text{Li}} - \mu_{\text{Li}}^*$ as variables. μ_{O}^* and μ_{Li}^* set the

Table 1: Lattice parameters and atomic charges of Cu, Cu₂O and Li₂O bulk phases in their hexagonal lattice.

	$a_h (\text{\AA})$	$c_h (\text{\AA})$	q_O	q_{Cu}	q_{Li}
Cu (<i>exp</i>) ¹⁸	5.12	6.27	-	-	-
Cu	5.12	6.32	-	0.0	-
Li ₂ O (<i>exp</i>) ¹⁸	6.53	8.00	-	-	-
Li ₂ O	6.58	8.06	-1.70	-	0.85
Cu ₂ O (<i>exp</i>) ¹⁹	6.04	7.40	-	-	-
Cu ₂ O ($U = 0$)	6.10	7.47	-1.06	0.53	-

upper limits of the phase diagram. They are defined as the DFT energies per atom in their standard state²⁹ : gaseous O₂ and metallic Li. To correct the well-known overbinding of the O₂ molecule within DFT formalism^{41,48} we compute a correction energy as done by Raddin *et al.*⁴⁹ which leads to an energy of -8.940 eV per O₂ molecule. The regions of the thermodynamic stability of Cu_xO_y phases were determined from formation energies computed using :

$$E_X^f = E_X^b - \sum_{j \in X} x_j \mu_j^* \quad (7)$$

where E_X^b is the bulk DFT energy per unit formula and x_j and μ_j^* are respectively the number of atoms in a unit formula and the chemical potential of specie j in its standard state. The results are presented in Table 2 at the PBE level.

Table 2: Calculated formation energies E_X^f at the PBE level.

compound	Cu ₂ O	CuO	Li ₂ O
E_X^f (eV/atom)	-5.985	-1.587	-1.692
exp (eV/atom)	-6.198	-1.631	-1.748

The phase diagram of {Cu, O, Li} is displayed Figure 4. As copper and copper oxide phases do not contain lithium atoms there is no dependence between $\Delta\mu_{\text{Li}}$ and $\Delta\mu_{\text{O}}$ and stability domains of these phases are represented as area. In the case of Li₂O, $\Delta\mu_{\text{Li}}$ and $\Delta\mu_{\text{O}}$ are not independent and Li₂O is stable only along a line. As the phase rule requires, chemical potential values for which two phases coexist are marked by lines and the crossings of two lines give thermodynamic conditions required in order to make three phases to coexist. Thus, on this diagram, the conversion processes of copper oxides along the electrochemical cycle follow the straight line corresponding to thermodynamic

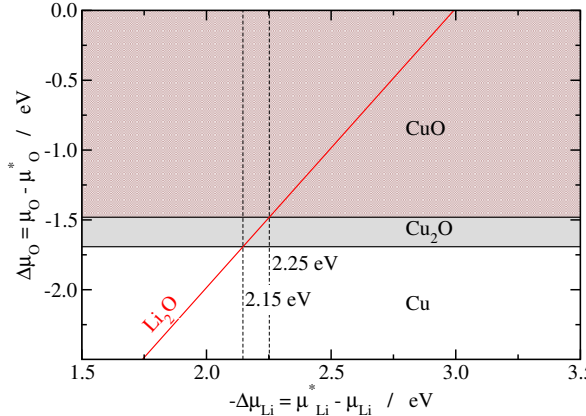


Figure 4: Phase diagram of $\{\text{Cu}, \text{O}, \text{Li}\}$ system at PBE level showing the stability regions of Cu_xO_y and Li_2O phases.

conditions for which Li_2O exists (red line on Figure 4). Cu_2O , Cu and Li_2O phases coexist at a voltage of 2.15 V against $\text{Li}|\text{Li}^+$ and CuO , Cu_2O and Li_2O coexist at a voltage of 2.25 V against $\text{Li}|\text{Li}^+$. These values agree well with experimental ones of 2.152 V and 2.321 V respectively.⁵⁰ In the following the relative stability of interface models will be investigated for a range of $-\Delta\mu_{\text{Li}}$ around 2.15 eV.

3.2 Commensurability of the phase

The 1×1 model was used in order to build the interface models and lattice parameters a_h are scaled until a perfect matching of the two lattices is reached. The a_h value was chosen such as the sum of the stress forces undergone along the a_h lattice parameter is zero. In that scope, potential energy surfaces, $PES_X(a_h, c_h)$ ($X = \text{Cu}, \text{Cu}_2\text{O}$ or Li_2O), were computed for a range of a_h and c_h values around the bulk equilibrium values. For each couple of a_h and c_h parameters the ion positions are relaxed. These calculations allow us to determine, for a given a_h , the value of c_h which relaxes the stress constraint. The top panel of Figure 5 shows the potential energy curves $E_X(a_h)$ along a_h (X is Cu , Cu_2O or Li_2O) which are sections of $PES_X(a_h, c_h)$ along the minimum energy path. Each point corresponds to a couple (a_h, c_h) for which when freezing a_h the energy is minimum.

From the derivatives of the potential energy curves, $E_X(a_h)$, the forces acting on a_h for each couple of phase ($\text{Cu}_2\text{O}-\text{Cu}$, $\text{Li}_2\text{O}-\text{Cu}$ and $\text{Cu}_2\text{O}-\text{Li}_2\text{O}$) were computed as the sum of the forces acting on a_h from each

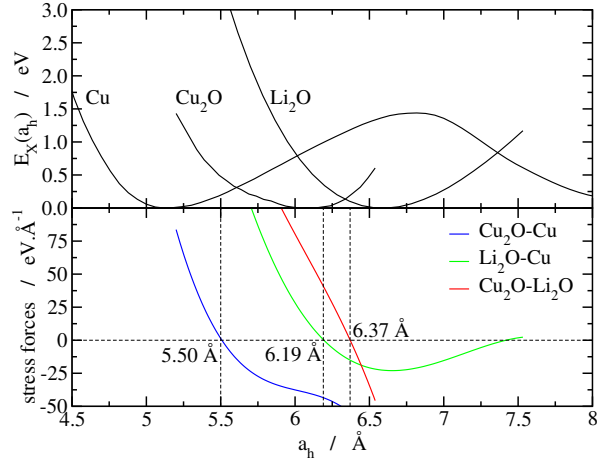


Figure 5: Top panel: potential energy curves $E_X(a_h)$ ($X = \text{Cu}, \text{Cu}_2\text{O}$ or Li_2O) as a function upon a_h . Each point correspond to a couple (a_h, c_h) for which the energy is minimum. Bottom panel: stress forces on a_h undergone by the interface models and computed following equation (8).

phase, weighted by the number of unit formula composing the interface model:

$$f_{A/B}(a_h) = -N_A \frac{dE_A(a_h)}{da_h} - N_B \frac{dE_B(a_h)}{da_h} \quad (8)$$

where N_A and N_B are the numbers of unit formula of phases A and B in the interface model, and $E_A(a_h)$ and $E_B(a_h)$ are respectively the sections of $PES_A(a_h, c_h)$ and $PES_B(a_h, c_h)$ along the minimum energy path. Here, only stoichiometric interface models were considered and they are composed as follow : $(\text{Cu}_2\text{O})_{16}-\text{Cu}_{28}$, $(\text{Li}_2\text{O})_{28}-\text{Cu}_{50}$ and $(\text{Cu}_2\text{O})_{14}-(\text{Li}_2\text{O})_{24}$. The resulting stress forces $f_{A/B}(a_h)$ are plotted Figure 5 bottom panel. For each interface, the a_h value corresponding to a zero force was used as a starting point before the full relaxation of the interface models, namely 5.50 Å for Cu₂O-Cu interfaces, 6.19 Å for Li₂O-Cu interfaces and 6.37 Å for Cu₂O-Li₂O interfaces.

Distortion of the lattice does not involve strong modifications on the electronic properties of the bulk. Densities Of States (DOS) of bulks Cu, Li₂O and Cu₂O are plotted on Figure 6 for optimized lattice parameters and for compressed or expanded structures at optimal a_h values. The position of the bands and the gap are not modified by the deformation of the lattice. The same observation can be done on atomic charges, see Table

3. The largest difference is 0.02e which is not a relevant deviation. These small modifications may be attributed to the fact that bulk distortions do not break chemical bonds. Indeed, while a_h increases or decreases by 3 to 10%, bond length elongation does not exceed 5%. For example, in the case of Cu_2O , when a_h decreases by about 10% bond length decreases by about only 2%.

Table 3: Lattice parameters and atomic charges of Cu, Cu_2O and Li_2O bulk phases in their hexagonal lattice with a_h values used to build interface models.

	a_h (Å)	c_h (Å)	q_O	q_{Cu}	q_{Li}
Li_2O	6.19	8.38	-1.69	0.84	
Li_2O	6.37	8.25	-1.70	0.85	
Cu	5.50	5.96			
Cu	6.19	5.26			
Cu_2O	5.50	8.67	-1.00	0.50	
Cu_2O	6.37	6.94	-1.02	0.51	

3.3 Relaxed structures

Using a_h parameters previously determined, all interface models were built and fully relaxed. In the case of $\text{Li}_2\text{O}-\text{Cu}$ interfaces, a_h increases from 6.19 Å to 6.25 Å ((Li_2O)Li–Cu) and 6.29 Å ((Li_2O)O–Cu). $\text{Cu}_2\text{O}-\text{Li}_2\text{O}$ interface models were built with $a_h = 6.37$ Å and relaxed structures exhibit a_h values between 6.35 and 6.42 Å. For $\text{Cu}_2\text{O}-\text{Cu}$ interfaces, a_h decreases from 5.50 Å to 5.40 Å (type 1) and 5.38 Å (type 2), see Figure 3 for type 1 and 2 interface models. The full relaxation of all systems does not change a_h by more than 2% and thus the strategy used for determining a_h seems to be well suited. Moreover, as the dispersion of relaxed a_h values is quite small, the distortion of bulk phases is similar in each interface models.

The deviation between the c_h parameter of each phase in the interface model and the c_h parameter in the corresponding bulks does not exceed 1%. Moreover, Bader charges analyses and DOS calculations show that the electronic properties of the distorted bulks are well conserved in the inner atomic planes. Thus, the length of each phase along the \vec{c} axis seems to be long enough in order to describe correctly the structural and electronic properties of bulk phases and to assume that the two interfaces of each model do not interact.

Actually, interfacial effects are strongly localised on the atomic layers composing the interface models. For example, in the case of (Li_2O)O–Cu, the atomic charge

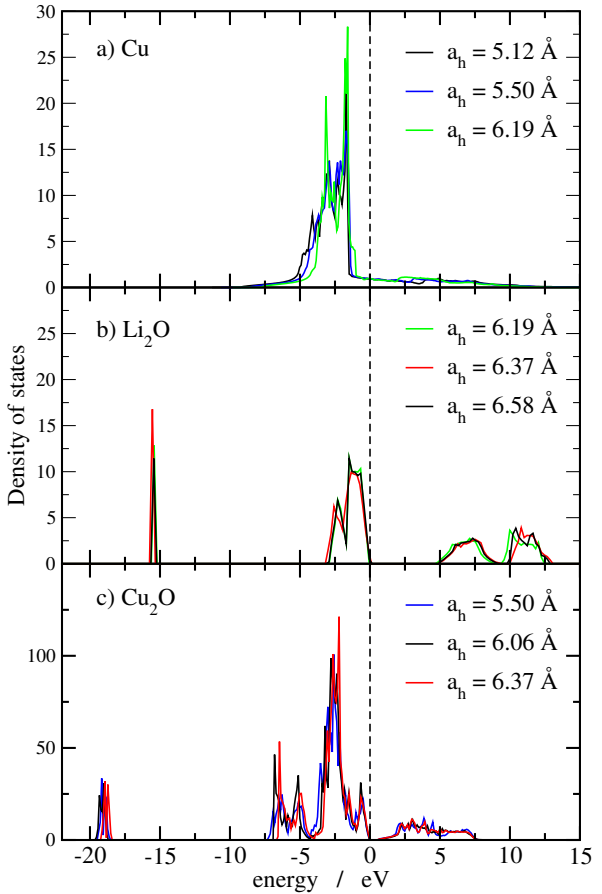


Figure 6: DOS for Cu_2O , Li_2O and Cu bulk phases at equilibrium lattice (in black) and for distorted lattices corresponding to the a_h values used to build interface models. DOS of a_h values corresponding to $\text{Cu}_2\text{O}-\text{Cu}$ interfaces are in blue, $\text{Li}_2\text{O}-\text{Cu}$ interfaces in green and $\text{Cu}_2\text{O}-\text{Li}_2\text{O}$ interfaces in red. Cu_2O DOS were computed at the PBE+U level with $U = 4$ eV.

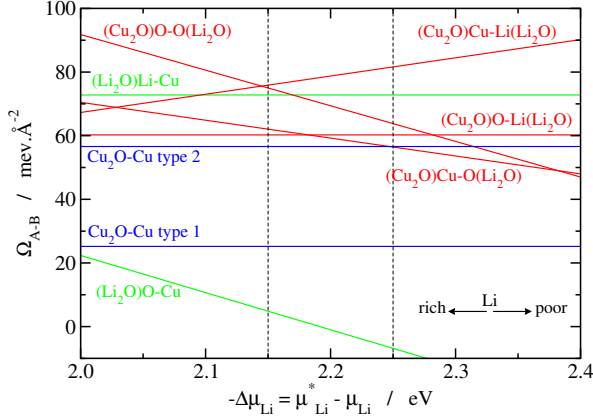


Figure 7: Grand potential Ω_{A-B} for each interface model as a function upon $\Delta\mu_{Li}$. Dashed vertical lines indicate the voltage against $LiLi^+$ for which Cu_2O , Cu and Li_2O coexist, *i.e.* 2.15 eV and the one for which CuO , Cu_2O and Li_2O coexist, *i.e.* 2.25 eV.

of copper and oxygen atoms at the interface are respectively $q_{Cu} = 0.49e$ and $q_O = -1.36e$. q_{Cu} is close to the atomic charge of a copper atom of Cu_2O , see Table 1. q_O is an intermediate value between the atomic charges of an oxygen atoms of Cu_2O and Li_2O , see Table 1 and is consistent with the fact that these oxygen atoms are bonded to three copper atoms and four lithium atoms, see Figure 3. Atomic charges of all other atoms do not exhibit relevant deviations from bulk values, Table 1. These observations can be generalized to all interface models.

3.4 Thermodynamic results

Using equations (4), (5) and (6), grand potentials were computed as a function upon $\Delta\mu_{Li}$ in a range of values consistent with the phase diagram, Figure 4. The results are shown on Figure 7 for the most probable interfaces at the PBE+ U level with $U = 4$ eV which seems more appropriated for thermodynamic investigations of copper oxide.⁴¹

Low values of $-\Delta\mu_{Li}$ correspond to Li-rich conditions whereas high values of $-\Delta\mu_{Li}$ correspond to Li-poor conditions. As Li and O atoms are in chemical equilibrium with Li_2O bulk phase, μ_{Li} and μ_O are not independent and O-rich and O-poor regions are inverted with respect to the Li-rich and Li-poor regions. As a consequence, oxygen rich interface models, such as $(Cu_2O)O-O(Li_2O)$, are stabilized at high values

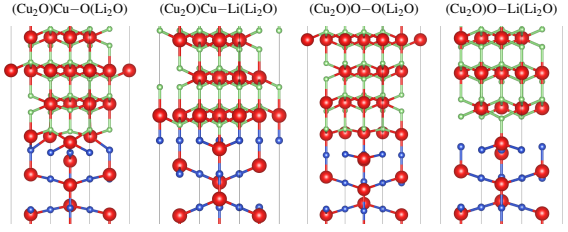


Figure 8: Most stable interface models among the Cu_2O – Li_2O interfaces projected in the (100) plane.

of $-\Delta\mu_{Li}$, whereas lithium rich interface models such as $(Cu_2O)Cu-Li(Li_2O)$ are stabilized at low values of $-\Delta\mu_{Li}$, see Figure 7.

In the case of Li_2O – Cu interfaces, the $(Li_2O)O-Cu$ is the most stable model which is not surprising because this is the only one model where oxygen atoms from the Li_2O part and copper atoms from the Cu part are directly face to face.

For Cu_2O – Cu interfaces, the most stable model is the type 1 model (see Figure 3 central picture for the structure). This may be the consequence of two factors. First, in the type 2 model, oxygen atoms are bonded to copper atoms on top sites whereas in the type 2 model, oxygen atoms are mainly on three fold sites and it was already observed that top sites are less stable than three fold sites.²⁷ Second, in the type 1 model the number of oxygen atoms at the interface is greater than in the type 2 model which leads to a larger number of Cu-O chemical bonds at the interface and stabilizes this interface model.

In the case of Cu_2O – Li_2O interfaces, the grand potential value is more dependent upon both the chemical composition of the interface and the lithium chemical potential. Nevertheless, the most stable models are those for which the atomic layers can make direct chemical bonds between O and Cu or Li atoms at the interface, *i.e.* $(Cu_2O)O-Li(Li_2O)$ and $(Cu_2O)Cu-O(Li_2O)$ models, see Figure 8. The relative stability of the $(Cu_2O)Cu-Li(Li_2O)$ and $(Cu_2O)O-O(Li_2O)$ interface models could be surprising and is due to interactions between the two last layers of each part, see Figure 8. Other interface models are less stable due to trivial reasons linked to electrostatic repulsions.

Figure 9 shows the effect of the U parameter upon the grand potential Ω_{A-B} for each interface model at $-\Delta\mu_{Li} = 2.15$ eV which corresponds to the coexistence of Cu_2O , Cu and Li_2O phases. Whatever the U value,

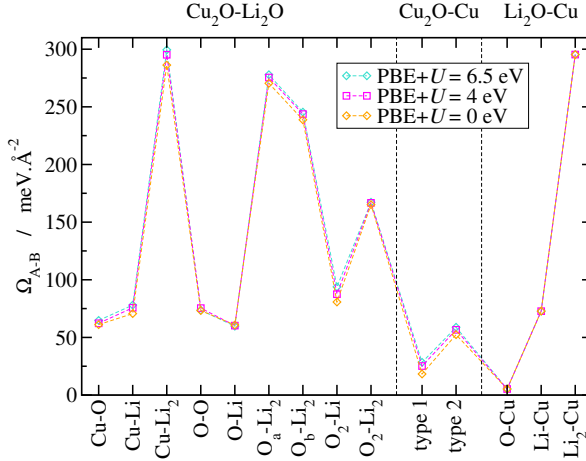


Figure 9: Effect of the U value upon the grand potential at $\Delta\mu_{\text{Li}} = -2.15 \text{ eV}$. The abscissa are the last atomic layers of each part of interface models. The index a and b for the $(\text{Cu}_2\text{O})\text{O}-\text{Li}_2(\text{Li}_2\text{O})$ interface models correspond respectively to a structure with oxygen atom on top sites or three fold sites upon the lithium atomic layer. $\text{Li}_2\text{O}-\text{Cu}$ interfaces are shown only for comparison (no U correction).

the order of the grand potential values is not modified.

From Figure 9, we can select the most stable interfaces which will be taken into account in order to discuss the structural behaviour of the electrode material. As Cu_2O , Cu and Li_2O phases coexist at $-\Delta\mu_{\text{Li}} = 2.15 \text{ eV}$, the most stable interface models were chosen at this chemical potential. The type 1 and the $(\text{Li}_2\text{O})\text{O}-\text{Cu}$ interface models are the most stable respectively for $\text{Cu}_2\text{O}-\text{Cu}$ and $\text{Li}_2\text{O}-\text{Cu}$ systems. In the case of $\text{Cu}_2\text{O}-\text{Li}_2\text{O}$ interfaces, two models have to be considered because their grand potential values are really close : $(\text{Cu}_2\text{O})\text{Cu}-\text{O}(\text{Li}_2\text{O})$ and $(\text{Cu}_2\text{O})\text{O}-\text{Li}(\text{Li}_2\text{O})$.

3.5 Structure of the conversion material

The calculations of grand potential as a function upon the voltage against $\text{Li}|\text{Li}^+$ have allowed us to identify the chemical composition of the most stable interfaces. In order to suggest a structural model of the electrode material, we will focus on the previously determined interfaces and we will assume that only those ones are formed in the material.

Usually, interface energies computed from theoretical methods are compared in the Young Dupré for-

malism to experimental measurements of wetting angle which are the only experimental probe of interface thermodynamics.^{3,4,6,7} These experiments consist of investigating the wetting behaviour of, for example, a molten metal upon a ceramic surface⁷ at high temperature. The case of conversion materials differs from wetting thermodynamics by two ways. First, the Young Dupré equation involves interfaces with a liquid or a gas phase which are not relevant in the present case because these phases do not exist in a conversion material. Second, in wetting investigations, we are looking at the expansion of a liquid drop upon the surface of a solid substrate at constant matter quantity whereas in conversion material, we are interesting in the behaviour of the material when phase transition occurs.

In this scope, our strategy is based on the comparison of the work of adhesion, W_{A-B}^{ad} between phases A and B composing the interface, and the work of self-adhesion of phases A and B, namely the opposite of the cleavage energies respectively called W_A^{ad} and W_B^{ad} , calculated for the same atomic termination of the interface. In a generalized case of the Dupré equation applied to all solid interfaces, the work of adhesion reads^{3,4}

$$W_{A-B}^{ad} = E_A^s + E_B^s - E_{A-B}^i \quad (9)$$

where E_{A-B}^i is the energy of the interface model and E_X^s ($X = A$ or B) are the energies of the slabs composing the interface model.

The work of adhesion is a positive quantity which gives the chemical affinity of two phases. The more W_{A-B}^{ad} is large the more phases A and B are bounded. Let us assume that the electrode is a composite material with phases A and B. Three situations are possible : (i) W_A^{ad} and W_B^{ad} are lower than W_{A-B}^{ad} , thus the growth of phase A on top of phase B and the formation of an interface is favoured contrary to the growth of phase A or B independently. Thus if one combines particles of phases A and B the whole system will tend to maximize the area of the interface between A and B ; (ii) on the contrary if W_A^{ad} and W_B^{ad} are greater than W_{A-B}^{ad} the formation of an interface between A and B is unfavoured and the system will tend to minimize the interface area between A and B ; (iii) if W_{A-B}^{ad} is included between W_A^{ad} and W_B^{ad} , the conclusion is not trivial and the resulting structure of the material cannot be clearly defined by this approach.

The works of adhesion and self-adhesion were calculated for the most stable interface models. The results are presented in Table 4 at the PBE+ U level, with

$U = 4$ eV. Calculations were also done with U values of 0 and 6.5 eV and once again, the U parameter does not change the relative order of W^{ad} . Thus the following discussion is available for all of the U parameter values used in this work. We will first discuss the structure of the electrode at the beginning and the end of the discharge of the material, then, we will discuss a more general situation.

At the end of the reduction of the material, the electrode contains Li_2O and Cu phases. According to W^{ad} values, we can guess that the formation of an interface between these two phases is favoured, see Table 4. Moreover, the fact that this interface show the lowest grand potential value support its stability whatever the voltage against $\text{Li}|\text{Li}^+$, see Figure 7. Although the values of $W_{(\text{Li}_2\text{O})\text{O}-\text{Cu}}^{ad}$ and $W_{\text{Li}_2\text{O}}^{ad}$ are close, the difference is still relevant. Indeed, in this system the area of the interface model in the plane of the interface is about 35 \AA^2 and the energy difference between these two works of adhesion is greater than 100 meV which is four times $k_B T$ at room temperature. As a consequence, Cu and Li_2O phases will tend to maximize their contact area, at least, until finite size effects become large. Thus at the end of the reduction, the electrode may look like small metallic copper particles dispersed into Li_2O . Experimentally, such a structure was already observed by TEM imaging microscopy for CuO electrode at this stage of the electrochemical cycle.¹⁵

At the beginning of the reduction, the electrode contains Cu_2O and Li_2O phases. According to W^{ad} values, see Table 4, the formation of the interface $(\text{Cu}_2\text{O})\text{Cu}-\text{O}(\text{Li}_2\text{O})$ is undefined whereas the formation of the interface $(\text{Cu}_2\text{O})\text{O}-\text{Li}(\text{Li}_2\text{O})$ is unfavoured. Moreover, the grand potential values of $\text{Cu}_2\text{O}-\text{Li}_2\text{O}$ interfaces are larger than grand potential values of other interfaces, see Figure 9, which suggests that Cu_2O and Li_2O interfaces are not favoured and will tend to minimize their area, or at least, Cu_2O and Li_2O will form large domains.

Now, if we consider an intermediate reduction state, the material is composed by particles of Cu_2O , Li_2O and Cu. Considering that at the beginning of the discharge, large Cu_2O domain are embedded into Li_2O the formation of the favoured $\text{Cu}_2\text{O}-\text{Cu}$ interfaces have to be considered, see Table 4. We can assume that Cu will appear at the interface between Li_2O and Cu_2O when an oxygen atom leaving the Cu_2O structure is trapped by Li^+ ions to form Li_2O . As the formation of $\text{Cu}_2\text{O}-\text{Cu}$ and $\text{Li}_2\text{O}-\text{Cu}$ interfaces are favoured, Cu will form

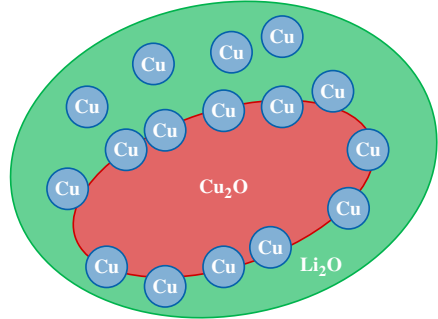


Figure 10: Schematic view of the electrode material.

small particles at the interface between Cu_2O and Li_2O . Then Cu particles will be progressively embedded into Li_2O all along the reduction process whereas Cu_2O phase will disappear, see Figure 10. The formation of Cu particles at the interface between Cu_2O and Li_2O may stabilize this interface and favour the conversion process.

4 Conclusion

In this paper, we have considered the formation of $\text{Cu}_2\text{O}-\text{Cu}$, $\text{Li}_2\text{O}-\text{Cu}$ and $\text{Cu}_2\text{O}-\text{Li}_2\text{O}$ interfaces in a conversion material. Starting from bulk phases, a complete investigation of all possible interface models was carried out at a *first principles* level. A grand canonical ensemble treatment allowed us to investigate the relative stability of interface models as a function upon the chemical composition of the interface and the voltage against $\text{Li}|\text{Li}^+$.

Considering a range of voltage against $\text{Li}|\text{Li}^+$ for which Cu_2O , Cu and Li_2O phases coexist, the most stable interface models were identified. They are characterized by the formation at the interface of chemical bonds between the two part composing the interface and interfacial effects are strongly localized on the two atomic layers around the interface. We showed that the U parameter does not have strong effects upon the relative stability of the interfaces.

For the most stable interface models, the work of adhesion between the two phases composing the interface were computed and compared to the work of self-adhesion of the same phases with the same termination. This approach allows us to determine if the formation of an interface is favoured or not and to suggest a struc-

Table 4: Work of adhesion and self-adhesion computed at the PBE+U level with $U = 4$ eV for the most stable interface models.

interface models	W_{A-B}^{ad} (meV. \AA^{-2})	W_A^{ad} (meV. \AA^{-2})	W_B^{ad} (meV. \AA^{-2})	interface formation
$\text{Cu}_2\text{O}-\text{Cu}$ type 1	160.8	101.7	85.3	favoured
$(\text{Li}_2\text{O})\text{O}-\text{Cu}$	258.4	254.4	79.5	favoured
$(\text{Cu}_2\text{O})\text{Cu}-\text{O}(\text{Li}_2\text{O})$	235.6	100.6	251.3	undefined
$(\text{Cu}_2\text{O})\text{O}-\text{Li}(\text{Li}_2\text{O})$	21.1	51.4	29.9	unfavoured

ture of the electrode material along the reduction process. Our results showed that $\text{Cu}_2\text{O}-\text{Cu}$ and $\text{Li}_2\text{O}-\text{Cu}$ interfaces are favoured whereas $\text{Cu}_2\text{O}-\text{Li}_2\text{O}$ interfaces are globally unfavoured. As a consequence, the general structure of the electrode consists of large domains of Cu_2O particles in a Li_2O matrix with smaller Cu particles embedded into Li_2O and at the $\text{Cu}_2\text{O}-\text{Li}_2\text{O}$ interface which may act as a surfactant and stabilize the $\text{Cu}_2\text{O}-\text{Li}_2\text{O}$ interface.

This work develops a first approach in order to investigate composite material or solid-solid interface issues by means of *first principles* calculations. The next step will be to built a more quantitative model in order to estimate the size of the particles and to take into account kinetic effects which can be strong in electrochemical processes.

Acknowledgments

This work was performed using HPC resources from GENCI-CINES (Grant 2012- c2012086920) and from the Mesocentre de Calcul Intensif Aquitain. Structural pictures were done with VESTA 3 software.⁵¹

References

- [1] H. Li, W. Zhang and J. R. Smith, *physica status solidi (a)*, 2011, **208**, 1166–1173.
- [2] S. Wang and H. Ye, *Current Opinion in Solid State and Materials Science*, 2006, **10**, 26–32.
- [3] S. B. Sinnott and E. C. Dickey, *Materials Science and Engineering: R: Reports*, 2003, **43**, 1–59.
- [4] E. Saiz, R. M. Cannon and A. P. Tomsia, *Annual Review of Materials Research*, 2008, **38**, 197–226.
- [5] F. Bottin and F. Finocchi, *Physical Review B*, 2007, **76**, 165427.
- [6] A. Hashibon, C. Elsässer, Y. Mishin and P. Gumbsch, *Physical Review B - Condensed Matter and Materials Physics*, 2007, **76**, 245434.
- [7] A. Hashibon and C. Elsässer, *Scripta materialia*, 2010, **62**, 939–944.
- [8] A.-L. Dalverny, J.-S. Filhol and M.-L. Doublet, *Journal of Materials Chemistry*, 2011, **21**, 10134–10142.
- [9] Y. Zhukovskii, P. Balaya, E. Kotomin and J. Maier, *Physical Review Letters*, 2006, **96**, 058302.
- [10] O. I. Malyi, Z. Chen, G. G. Shu and P. Wu, *Journal of Materials Chemistry*, 2011, **21**, 12363.
- [11] E. Peled, *Journal of The Electrochemical Society*, 1979, **126**, 2047.
- [12] P. Poizot, S. Laruelle, S. Gruegeon, L. Dupont and J.-M. Tarascon, *Nature*, 2000, **407**, 496–499.
- [13] R. Malini, U. Uma, T. Sheela, M. Ganesan and N. Renganathan, *Ionics*, 2009, **15**, 301–307.
- [14] J. Cabana, L. Monconduit, D. Larcher and M. R. Palacín, *Advanced Materials*, 2010, **22**, E170–E192.
- [15] A. Debart, L. Dupont, P. Poizot, J.-B. Leriche and J. Tarascon, *Journal of the Electrochemical Society*, 2001, **148**, A1266–A1274.
- [16] S. Gruegeon, S. Laruelle, R. Herrera-Urbina, L. Dupont, P. Poizot and J.-M. Tarascon, *Journal of the Electrochemical Society*, 2001, **148**, A285–A292.
- [17] S. Hibble, C. Malitesta and P. Dickens, *Solid State Ionics*, 1990, **39**, 289–295.
- [18] R. W. G. Wyckoff, *Crystal Structures*, Second edition. Interscience Publishers, New York, 1965.

- [19] A. Werner and H. D. Hochheimer, *Physical Review B*, 1982, **25**, 5929–5934.
- [20] A. Soon, M. Todorova, B. Delley and C. Stampfl, *Phys. Rev. B*, 2007, **75**, 125420.
- [21] K. Schulz and D. Cox, *Physical Review B*, 1991, **43**, 1610–1621.
- [22] N. Seriani, *Nanotechnology*, 2009, **20**, 445703.
- [23] L. Liu, V. E. Henrich, W. P. Ellis and I. Shindo, *Phys. Rev. B*, 1996, **54**, 2236–2239.
- [24] J. Kunze, V. Maurice, L. Klein, H.-H. Strehblow and P. Marcus, *Journal of Physical Chemistry B*, 2001, **105**, 4263–4269.
- [25] L. Liu, S. Wang and H. Ye, *Surface and Interface Analysis*, 2003, **35**, 835–841.
- [26] H. Dai, J. Du, L. Wang, C. Peng and X. Liu, *Physica B: Condensed Matter*, 2010, **405**, 573–578.
- [27] K. Radican, N. Berdunov, G. Manai and I. Shvets, *Physical Review B - Condensed Matter and Materials Physics*, 2007, **75**, 155434.
- [28] X.-G. Wang and J. R. Smith, *Physical Review Letters*, 2005, **95**, 156102.
- [29] W. Zhang, J. R. Smith and X. Wang, *Physical Review B*, 2004, **70**, 024103.
- [30] G. Kresse and J. Hafner, *Phys. Rev. B*, 1993, **47**, 558–561.
- [31] G. Kresse and J. Furthmüller, *Computational Materials Science*, 1996, **6**, 15 – 50.
- [32] J. P. Perdew, K. Burke and M. Ernzerhof, *Phys. Rev. Lett.*, 1996, **77**, 3865–3868.
- [33] P. E. Blöchl, *Phys. Rev. B*, 1994, **50**, 17953–17979.
- [34] G. Kresse and D. Joubert, *Phys. Rev. B*, 1999, **59**, 1758–1775.
- [35] S. L. Dudarev, G. A. Botton, S. Y. Savrasov, C. J. Humphreys and A. P. Sutton, *Phys. Rev. B*, 1998, **57**, 1505–1509.
- [36] V. Anisimov, J. Zaanen and O. Andersen, *Physical Review B*, 1991, **44**, 943–954.
- [37] V. Anisimov, F. Aryasetiawan and A. Lichtenstein, *Journal of Physics Condensed Matter*, 1997, **9**, 767–808.
- [38] J. Hu, D. Li, J. G. Lu and R. Wu, *The Journal of Physical Chemistry C*, 2010, **114**, 17120–17126.
- [39] D. Wu, Q. Zhang and M. Tao, *Physical Review B - Condensed Matter and Materials Physics*, 2006, **73**, 235206.
- [40] M. Nolan and S. Elliott, *Physical Chemistry Chemical Physics*, 2006, **8**, 5350–5358.
- [41] L. Wang, T. Maxisch and G. Ceder, *Physical Review B - Condensed Matter and Materials Physics*, 2006, **73**, 195107.
- [42] W. Tang, E. Sanville and G. Henkelman, *Journal of Physics Condensed Matter*, 2009, **21**, 084204.
- [43] G. Henkelman, A. Arnaldsson and H. c. Jonsson, *Computational Materials Science*, 2006, **36**, 354–360.
- [44] M. Islam, B. Diawara, V. Maurice and P. Marcus, *Journal of Molecular Structure: THEOCHEM*, 2009, **903**, 41–48.
- [45] M. Islam, B. Diawara, V. Maurice and P. Marcus, *Surface Science*, 2009, **603**, 2087–2095.
- [46] Y. Xu and W. Shelton, *Journal of Chemical Physics*, 2010, **133**, 024703.
- [47] D. Kramer and G. Ceder, *Chem. Mater.*, 2009, **21**, 3799–3809.
- [48] S. Kurth, J. P. Perdew and P. Blaha, *International Journal of Quantum Chemistry*, 1999, **75**, 889–909.
- [49] M. D. Radin, J. F. Rodriguez, F. Tian and D. J. Siegel, *J. Am. Chem. Soc.*, 2011, **134**, 1093–1103.
- [50] *Lithium batteries*, ed. J. Gabano, Academic Press, London ; New York (N. Y.) ; Paris [etc.], 1983.
- [51] K. Momma and F. Izumi, *Journal of Applied Crystallography*, 2011, **44**, 1272–1276.